Available online at www.sciencedirect.com
SCIENCE DIRECT®
C. R. Physique 4 (2003) 555–570
COMPTES RENDUS PHYSIQUE

Exotic nuclei/Les noyaux exotiques

Mean field theories and exotic nuclei

Karim Bennaceur [a], Paul Bonche [b], Jacques Meyer [a,*]

[a] *Institut de physique nucléaire de Lyon, CNRS-IN2P3/Université Claude Bernard Lyon 1, bâtiment Paul Dirac, 43, Bd. 11.11.18, 69622 Villeurbanne cedex, France*
[b] *Service de physique théorique, CEA Saclay, 91191 Gif-sur-Yvette cedex, France*

Presented by Guy Laval

Abstract

A general description of mean field theories is made in view of their use for the description of static and dynamical properties of exotic nuclei. Some pertinent examples of new physics appearing far from stability are presented such as quenching of shell effects around the neutron drip line as well as the effect of the continuum in Hartree–Fock–Bogoliubov formalism when the Fermi energy goes to zero. We also focus on the effective forces adjusted to investigate nuclear medium in these particular extreme conditions. Some perspectives of new theoretical developments are suggested in order to guarantee the reliability of future predictions in this new field of physics. ***To cite this article: K. Bennaceur et al., C. R. Physique 4 (2003).***

Résumé

Théories de champ moyen et noyaux exotiques. Après une présentation générale des théories de champ moyen, on s'attache plus spécifiquement à l'étude de quelques applications originales dans le domaine des noyaux exotiques. Les principales hypothèses de ces modèles sont discutées vis-à-vis des conditions extrêmes de ce nouveau champ d'application. Quelques perspectives sont suggérées ouvrant la voie de développements théoriques futurs indispensables à ce domaine de noyaux très loin de la stabilité. ***Pour citer cet article : K. Bennaceur et al., C. R. Physique 4 (2003).***

Keywords: Mean field; Hartree–Fock; Hartree–Fock–Bogoliubov; Generator coordinate method

Mots-clés : Champ moyen ; Hartree–Fock ; Hartree–Fock–Bogoliubov ; Coordonnée génératrice

1. Introduction

Microscopic theories using the mean field approximation have been gaining, year after year, a high level of reliability for the description of static and dynamic properties of atomic nuclei. Reasonable theoretical predictions can now be expected to explain the properties of nuclei not only in their ground states but also in extreme conditions of spin or isospin far away from the normal stability of the nuclear matter.

Static properties essentially involve ground states of nuclei – binding energies, radii, separation energies of one or two nucleons, shell effects… – and are well described within Hartree–Fock or Hartree–Fock–Bogoliubov approaches including pairing correlations. Dynamic properties more generally affect the excited states – single or collective excitations, giant resonances, fission… – for which it is necessary to go beyond the mean field approximation in order to obtain a correct description of experimental data. These methods, such as the random phase approximation or the generator coordinate method,

* Corresponding author.
E-mail address: jmeyer@ipnl.in2p3.fr (J. Meyer).

1631-0705/03/$ – see front matter
doi:10.1016/S1631-0705(03)00060-4

perform a particular mixing of configurations. And to be consistent they are all based on a set of wave functions issued from a mean field calculation and in this way they can be generated as successive approximations of the general Time-Dependent Hartree–Fock formalism.

Whether nonrelativistic, i.e., formulated with the Schrödinger equation or relativistic, i.e., using the Dirac equation [1], all these models are using an *effective interaction* (or an *effective Lagrangian*) as a basic input which is generally built in a phenomenological way. The *effective* feature must be considered as a way to bypass the main theoretical difficulties occurring in ab initio calculations starting from realistic free nucleon–nucleon interaction. These effective forces follow some criteria of simplicity and their parameters are determined *once and for all* to describe some bulk properties of the nuclear matter. The oldest parametrizations of these effective interactions were determined from spherical nuclei in the valley of stability. However in the new physics of these extreme conditions recently occurring thanks to radioactive beam facilities [2], one is bound to reconsider these parametrizations.

2. A microscopic mean field theory: the Hartree–Fock theory

Microscopic mean field theories are based on the fundamental assumption that neutrons and protons inside the nucleus are moving independently from each other under the influence of a potential averaging their interactions. This approximation finds a steady experimental verification for instance in the shell model framework and the occurrence of magic numbers. A simple calculation [3,4] enables to justify this approximation when evaluating the mean free path of a nucleon inside the nucleus which turns out to be several times larger than the size of the nucleus. The explanation of this result is that the Pauli principle limits strongly the possible final states in case of nucleon–nucleon collisions in the nucleus. As a matter of fact a nucleon does not see the other ones but only feels the average potential which retains it inside the nucleus.

Beside the shell model, a mean field theory enables to derive the nuclear mean field microscopically. The main basic ingredient is a microscopic Hamiltonian (hereafter non relativistic) which uses an effective two-body nucleon–nucleon (NN) interaction V_{ij}^{eff}:

$$H = K + V = \sum_{i=1}^{A} \frac{\mathbf{p}_i^2}{2m} + \frac{1}{2} \sum_{i \neq j=1}^{A} V_{ij}^{\text{eff}}. \tag{1}$$

In the Hartree–Fock method (HF), the ground state wave function of the nucleus is approximated by a Slater determinant built on single-particle wave functions within the independent particle picture:

$$\Psi_{\text{HF}}(\boldsymbol{r}_1, \ldots, \boldsymbol{r}_A) = \frac{1}{\sqrt{A!}} \det\bigl\{\phi_{\alpha_1}(\boldsymbol{r}_1) \cdot \phi_{\alpha_2}(\boldsymbol{r}_2) \cdots \phi_{\alpha_A}(\boldsymbol{r}_A)\bigr\}. \tag{2}$$

The single-particle orbitals ϕ_α are obtained by minimization of the total energy of the nucleus:

$$E_{\text{HF}} = \frac{\langle \Psi_{\text{HF}} | H | \Psi_{\text{HF}} \rangle}{\langle \Psi_{\text{HF}} | \Psi_{\text{HF}} \rangle}. \tag{3}$$

This variational principle leads to the system of Hartree–Fock equations [5]:

$$h\phi_{\alpha_i} = \left\{ -\frac{\hbar^2}{2m} \nabla^2 + U_{\text{HF}}[\phi_\alpha] \right\} \phi_{\alpha_i} = \varepsilon_{\alpha_i} \phi_{\alpha_i}, \quad i = 1, \ldots, A, \tag{4}$$

where the HF mean field $U_{\text{HF}}[\phi_\alpha]$ itself depends upon the single-particle wave functions ϕ_α generating thus a self-consistent system of A nonlinear equations. This system can there be rewritten using the local part of the nucleon density matrix ($\rho(\boldsymbol{r}, \boldsymbol{r}') = \sum_{i=1}^{A} \phi_{\alpha_i}^*(\boldsymbol{r}) \phi_{\alpha_i}(\boldsymbol{r}')$) in the case of a zero range force:

$$\rho(\boldsymbol{r}, \boldsymbol{r}) = \rho(\boldsymbol{r}) \quad \Rightarrow \quad \bigl[h, \rho(\boldsymbol{r})\bigr] = 0 \quad \Rightarrow \quad \phi_\alpha,\ \varepsilon_\alpha,\ U_{\text{HF}}[\phi_\alpha]. \tag{5}$$

The self-consistent system of HF equations (Eq. (4)) is generally solved by iterations giving, at convergence, a set of single-particle wave functions ϕ_α, their energies ε_α and the HF mean field $U_{\text{HF}}[\phi_\alpha]$. This system of $A = N + Z$ equations is solved for all the A nucleons (Z protons + N neutrons) without any "inert core". It does not contain any parameter fitted afterwards on experimental data. Results such as masses, radii, binding energies... are then directly comparable to experiment. The sole ingredient is the *effective interaction* V_{ij}^{eff}. This interaction is built once for all following a well defined protocol.

With constraints, one can analyze the nucleus out of its ground state, seeking for instance shape isomers [6–11]. Fig. 1 displays an example of constrained HF (CHF) calculations for Magnesium isotopes where an axial quadrupole moment constraint $Q = Q_{20} = r^2 Y_{20}$ enables to follow the energy of the nucleus as a function of this degree of freedom. Different minima occur for these Magnesium isotopes: a spherical shape for ^{20}Mg and ^{32}Mg; a prolate one weakly deformed for

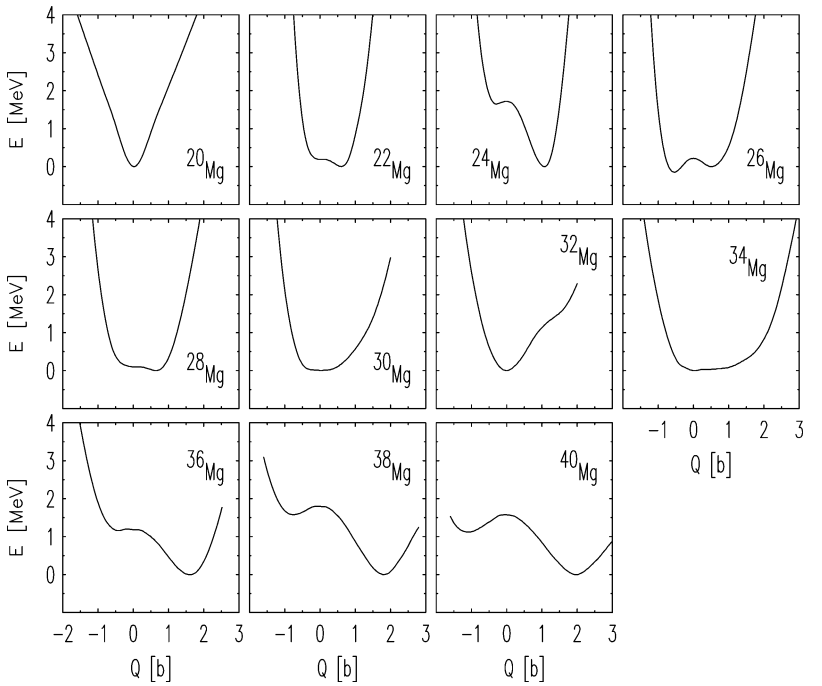

Fig. 1. Deformation energies curves for the even–even Magnesium isotopes $^{20-40}$Mg obtained within CHF calculations using the Skyrme SIII effective force [28]. The deformation potential energies are plotted as a function of the axial deformation analyzed in terms of the mass quadrupole moment of the nucleus. The ground state of each nucleus is taken as the origin of the energies. This figure is reprinted from Terasaki et al. [12], with permission from Elsevier.

^{24}Mg, and a more deformed one for exotic neutron rich nuclei ^{36}Mg to ^{40}Mg for which two prolate and oblate minima are in competition [12].

Fig. 2 displays some examples of the variety of shapes obtained with CHF calculations for $N = Z$ nuclei with two constraints on quadrupole moments Q_{20} and Q_{22}. The axial and triaxial deformations are thus investigated and the potential energy surfaces are plotted using the usual $\{\beta, \gamma\}$ representation. For the doubly magic ^{100}Sn nucleus one obtains a spherical shape whereas more complex shapes occur for lighter nuclei: a competition between spherical and highly deformed shapes for the ^{80}Zr nucleus; an oblate shape for the ^{72}Kr; a specific shape which is not precisely defined between spherical and weakly deformed for the ^{60}Zn, ^{52}Fe and ^{48}Cr nuclei. In these cases, dynamical calculations beyond the mean field approximation will be required to obtain the true ground state stable against quantum quadrupole fluctuations (see Section 3.3).

Fig. 3 shows the result of a double constrained CHF calculation both on the axial quadrupole and octupole moments for the ^{194}Pb nucleus. The potential energy surface is then plotted as a function of the axial quadrupole Q_{20} and octupole $Q_{30} = r^3 Y_{30}$ moments. One can see clearly a spherical absolute minimum for the ground state of this nucleus and two other minima for large prolate deformations: one second minimum, generating the superdeformed states, characterized by a strong octupole softness which is responsible of the asymmetric fission in the case of the actinides; and even a third minimum, possibly for the hyperdeformed states?

3. The effective interaction for mean field theories

The old problem of the determination of realistic nucleon–nucleon (NN) force (V in Eq. (1)) remains the key point of the whole hadronic physics dedicated to the study of the static and dynamic properties of atomic nuclei. Since almost seventy years, tremendous works has been developed to construct interactions to describe free NN scattering and some few nucleons bound states. All these forces have to be renormalized to describe the interaction of nucleons inside the nucleus where the Pauli principle limits strongly the final states during a two-body collision. The concept of *effective interaction* enables to overcome this problem in a phenomenological way.

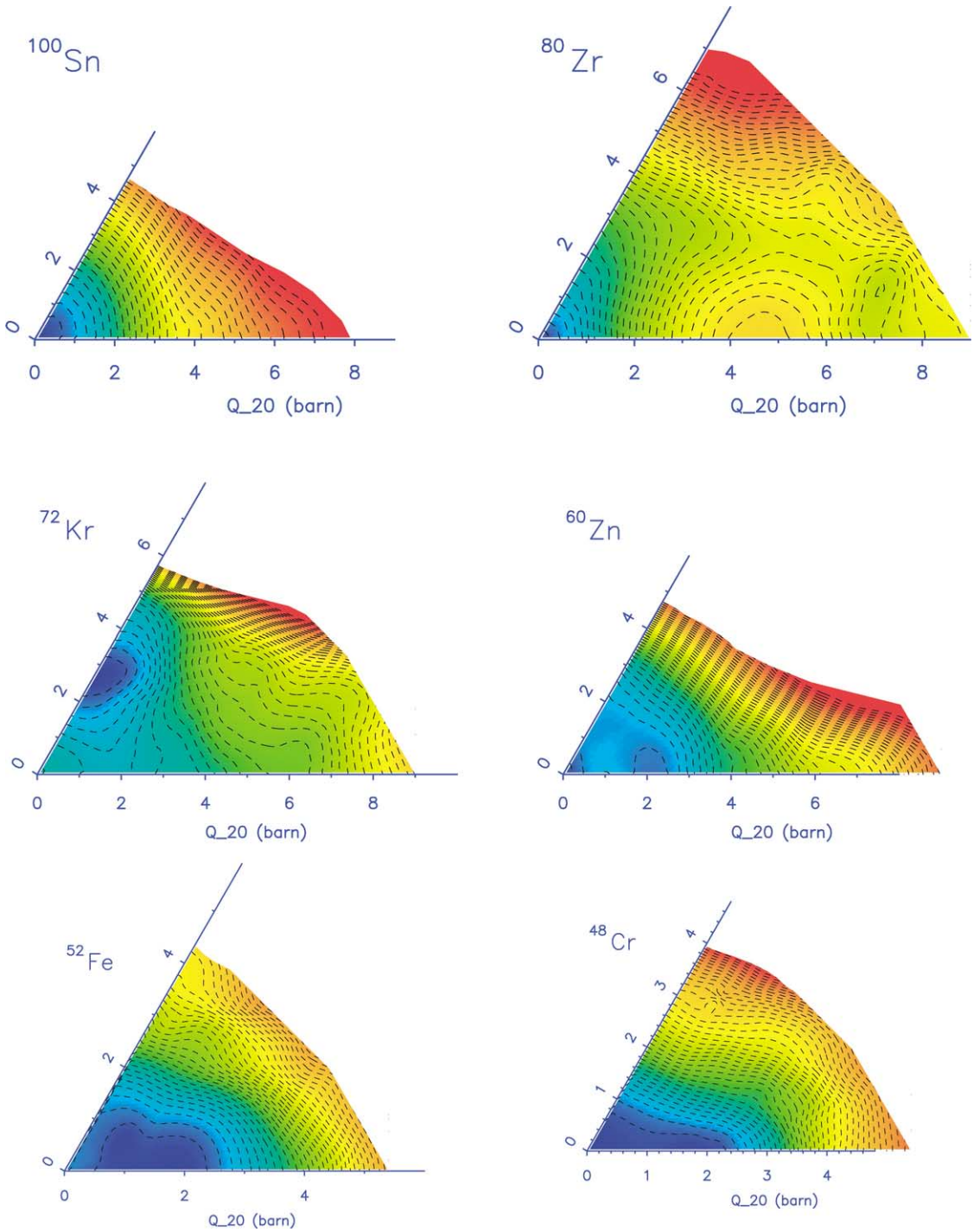

Fig. 2. Potential energy surfaces for some $N = Z$ nuclei obtained in CHF calculations and projection onto neutron and proton numbers. The SLy4 effective force is used. The energy is plotted as a function of the axial quadrupole moment Q_{20} and the triaxial Q_{22} moment which is parametrized using the γ angle. Prolate shapes correspond to $\gamma = 0$, oblate shapes to $\gamma = 60°$ and triaxial shapes to other values of γ. The ground state energy is taken as the origin of the energies and the distance between two isocontours corresponds to 0.4 MeV.

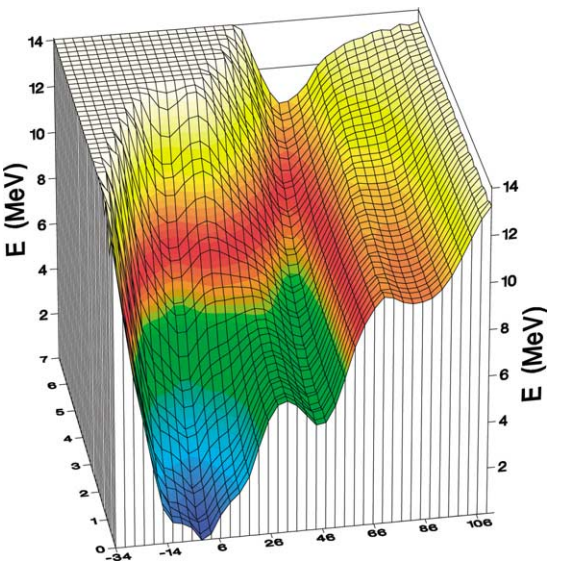

Fig. 3. Potential energy surface of the ^{194}Pb nucleus obtained in a CHF calculation using two constraints. The energy is plotted as a function of the axial quadrupole (-34 b $< Q_{20} < +106$ b) and octupole ($0 < Q_{30} < 7000$ fm^3) moments. The ground state energy is taken as the origin of the energies. This figure is reprinted from Meyer et al. [13], with permission from Elsevier.

In perturbative approaches of nuclear matter, a realistic free NN interaction is generally tested in symmetric infinite nuclear matter within the Brueckner–Hartree–Fock (BHF) formalism. It consists in the construction of a G matrix solution of the Bethe–Goldstone equations [3,14] which can be written as:

$$G = V - V\frac{Q}{e}G = V - V\frac{Q}{e}V\frac{Q}{e}V + \cdots, \tag{6}$$

where Q is the Pauli operator eliminating occupied intermediate states and e is the energy denominator. The total energy takes the same form as in the HF approximation except that the G matrix elements are replacing the 2-body matrix elements of the interaction V:

$$E = \sum_i \frac{\hbar^2 k_i^2}{2m} + \frac{1}{2}\sum_{ij<F}\langle ij|G(E = e_i + e_j)|ij\rangle, \tag{7}$$

where the single-particle energies e_i are self-consistently defined at the lowest order of the G matrix expansion:

$$e_i = \frac{\hbar^2 k_i^2}{2m} + \sum_{j<F}\langle ij|G(E = e_i + e_j)|ij\rangle. \tag{8}$$

For all realistic interactions, this order of approximation does not give a good convergence of the expansion (Eq. (6)) and higher order contributions are required [3,15–18]. This situation is summarized with Fig. 4 where each symbol denotes the saturation point of the symmetric infinite nuclear matter obtained at the lowest order for different realistic interactions. All these points are lying on a line known as the *Coester line* [19] far from the expected *empirical point* obtained from a liquid drop expansion of the energy per particle. Taking into account higher order terms [19], a new *Coester line* can be defined closer to the expected equilibrium. In finite nuclei where the construction of a G matrix implies further approximations [16,20,21], the situation is essentially the same [22].

An effective interaction [3,16,21,23] can be viewed as a phenomenological NN force which reproduces the main properties of infinite nuclear matter especially the saturation point. This effective force play the role of a G matrix, its matrix elements replace the G matrix elements in Eq. (7). The general form and the parameters of the effective force contain higher order terms and it is essential to exhibit the connection between pertinent terms of the force and specific properties of the nuclear fluid. One can show for instance that taking into account medium effects, such as the Pauli blocking, will result in a density dependence of the effective force.

There are two main groups of effective NN forces: finite range such as Gogny forces [24,25] or zero range such as Skyrme interactions [26–31]. Both of them have a simple analytical form and involve a limited number of parameters determined on the bulk properties of the nuclear matter and some nuclear data.

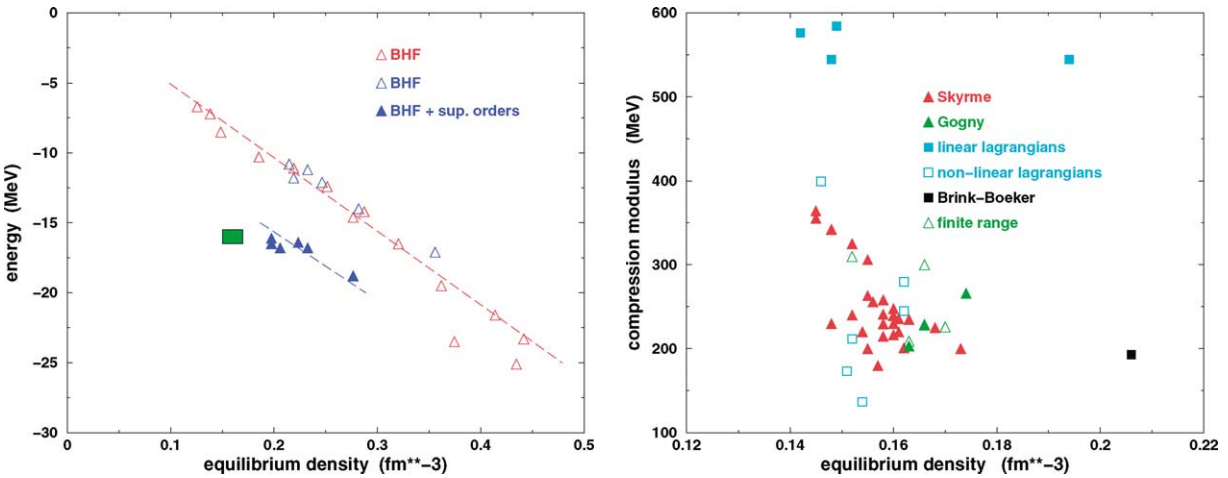

Fig. 4. Left: energy per particle for symmetric nuclear matter as a function of the equilibrium density for a different realistic NN interactions in BHF formalism. The empirical equilibrium point is marked by a green rectangle. Empty triangles (red and blue ones) give the results of lowest order BHF calculation. For some interactions (empty blue triangles), calculations have also been done including higher order terms (filled blue triangles).

Right: correlation between the compression modulus and the equilibrium density for a symmetric nuclear matter. The points represent different nonrelativistic effective interactions and relativistic effective Lagrangian: red triangles: zero range Skyrme forces; filled green triangles: finite range Gogny forces; empty green triangles: other finite range forces; black square: finite range Brink–Boeker force; filled blue squares: relativistic Lagrangian with linear coupling; empty blue squares: relativistic Lagrangian with nonlinear coupling.

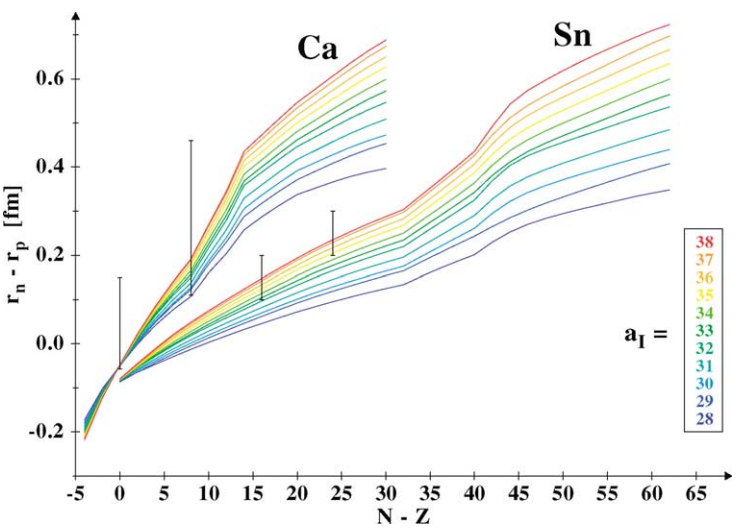

Fig. 5. Differences $r_n - r_p$ (in fm) between neutron and proton radii along the two isotopic series of Calcium and Tin. Spherical HFB calculations are performed using Skyrme effective forces based on a standard SLy4-like parametrization [31] except that the symmetry energy is varied from 28 to 38 MeV. The experimental data (vertical bars) are taken from Batty et al. [34].

These calculations are shown on the right of Fig. 4 in a plane defined by the compression modulus K_∞, related to the curvature of the energy per particle at saturation, and the equilibrium density ρ_0. The dispersion of the points indicates that there is a correlation between these two quantities [32]. Negele and Vautherin [33] have shown that higher order contributions in the G matrix expansion implies a density dependence of the interaction. This is confirmed by Fig. 4 where the points are gathered around the standard values of K_∞ and ρ_0 with the exception of Brink–Boeker forces which do not include such a density dependence. The same consideration applies to effective relativistic Lagrangian without nonlinear coupling with the σ meson, whose main effects is to simulate the same higher order terms.

Similarly to K_∞ which characterizes the curvature of the nuclear matter equation of state (EOS), the symmetry energy, which is the $(N-Z)/A$ coefficient in the Bethe–Weiszäcker mass formula, is the curvature of this EOS with respect to the isospin degree of freedom. It is the relevant parameter governing the properties of asymmetric nuclear matter and thus for the physics of exotic neutron rich nuclei. Fig. 5 shows the connection between this symmetry energy (a_I) and the difference between neutron and proton radii in two isotopic series of Calcium and Tin nuclei for SLy4-like [31] forces for different values of a_I. The comparison of the behavior of the differences $r_n - r_p$ with experiment suggests that the symmetry energy could be used to constrain the parameters of effective interactions. However, such a procedure requires more experimental data especially neutron radii which are actually too badly known to be used. In Calcium isotopes, the two radii which are known cannot constrain the symmetry energy, the error bars are much too large. In the case of Tin isotopes, the forces with $a_s \lesssim 35$ MeV seem to be excluded. However, correlations beyond the mean field approximation should be explored before drawing any definite conclusions.

3.1. Pairing correlations and the Hartree–Fock–Bogoliubov theory

The Hartree–Fock approximation is well adapted for the description of doubly closed shell nuclei where there is a large energy gap between the last occupied and the first unoccupied single-particle states. This gap guarantees the stability of a nucleus with magic numbers of nucleons. However, the HF approximation cannot describe mid-shell nuclei where no gap exists generating a ground state wave function which is degenerated with particle hole configurations. To construct a correct ground state wave function, it is necessary to take into account pairing correlations responsible for instance for several experimental signatures such as: (i) experimental specific spectra for even–even nuclei versus even–odd nuclei; (ii) even–odd effect giving generally a weaker binding energy for an odd nucleus than the arithmetic average of the neighbors even–even nuclei; (iii) collective vibrational character of the first 2^+ states for the even–even nuclei close to magic nuclei; (iv) difference in the height of the fission barriers of ^{235}U and ^{238}U nuclei.

The Hartree–Fock–Bogoliubov method [3] (HFB) takes into account self-consistently these pairing correlations. Let us start from the HF ground state wave function which can be written for an even–even nucleus as:

$$|\Psi_{\mathrm{HF}}\rangle = a^+_{\alpha_1} a^+_{\bar{\alpha}_1} a^+_{\alpha_2} a^+_{\bar{\alpha}_2} \cdots |0\rangle, \tag{9}$$

where a^+_α creates one nucleon in the ϕ_α state whereas $a^+_{\bar{\alpha}}$ creates one nucleon in the time reversed $\phi_{\bar{\alpha}}$ state and where the $|0\rangle$ state is a vacuum of particle. In the HFB formalism one uses a simplified pair wave function of correlated nucleons [35]. The independent particle HF state ($\{a, a^+\}$) becomes an independent quasi-particle HFB state ($\{\eta, \eta^+\}$) through the Bogoliubov–Valatin transformation:

$$\begin{pmatrix} \eta \\ \eta^+ \end{pmatrix} = B \begin{pmatrix} a \\ a^+ \end{pmatrix} = \begin{pmatrix} U & V \\ V^* & U^* \end{pmatrix} \begin{pmatrix} a \\ a^+ \end{pmatrix}. \tag{10}$$

The HFB ground state is now a vacuum of quasi-particles. The HF ρ density (Eq. (5)) becomes an HFB generalized density calculated from the normal and abnormal (pairing tensor) densities:

$$R = \begin{pmatrix} \rho & -\kappa \\ \kappa^* & 1-\rho^* \end{pmatrix}, \quad \rho = V^* V^{\mathrm{T}}, \quad \kappa = V^* U^{\mathrm{T}}. \tag{11}$$

The vectors $\{U, V\}$ are obtained by minimizing the total energy:

$$E_{\mathrm{HFB}} = \frac{\langle \Psi_{\mathrm{HFB}} | H | \Psi_{\mathrm{HFB}} \rangle}{\langle \Psi_{\mathrm{HFB}} | \Psi_{\mathrm{HFB}} \rangle}, \tag{12}$$

which leads to the following HFB system of equations:

$$B\mathcal{H} = EB, \quad \mathcal{H} = \begin{pmatrix} h & \Delta \\ -\Delta^* & -h^* \end{pmatrix}, \tag{13}$$

where the HF mean field h (Eq. (4)) is calculated with the ρ density (Eq. (11)) while the pairing field Δ takes the form:

$$\Delta_{\alpha\gamma} = \frac{1}{2} \sum_{\beta\delta} \langle \alpha\gamma | V^{\mathrm{eff}} | \beta\delta \rangle \kappa_{\delta\beta}. \tag{14}$$

The Ψ_{HFB} state does not have a fixed number of particles and it is necessary to introduce a constraint on the nucleon numbers (protons and neutrons) in the previous HFB system (Eq. (13)). The h HF mean field is replaced by $h - \lambda_N \widehat{N} - \lambda_Z \widehat{Z}$, where $\widehat{N}$ and $\widehat{Z}$ are the number of particle operators and λ_q the corresponding Lagrange multipliers. A more accurate protocol to control the number of particles in the HFB formalism can be made when adding a second order constraint on $\widehat{N}^2$ ($\widehat{Z}^2$ respectively) in the HF field as proposed by Lipkin and Nogami [36]. Such a prescription (denoted hereafter HFBLN or HFBCSLN) which includes

corrections to the total energy of the nucleus and to all one-body observables have been implemented by many authors [37]. It can be also used to generate a set of wave functions to perform first an exact projection onto the particle number and second a study of quantum fluctuations along a collective coordinate using the Generator Coordinate Method (GCM) [38] (see Section 3.3).

The Δ pairing field generally couples ϕ_α and $\phi_{\bar{\beta}}$ states with $\alpha \neq \beta$. The BCS approximation consists in neglecting the nondiagonal elements of Δ, i.e., in imposing solutions that couple only time reversed α and $\bar{\alpha}$:

$$U_\alpha = u_\alpha \phi_\alpha, \qquad V_\alpha = -v_\alpha \phi^*_{\bar{\alpha}}. \tag{15}$$

The HFB system simplifies in two steps:

- first by solving an HF problem to generate the set $\{\phi_\alpha, \varepsilon_\alpha\}$,
- second by solving the well-known "gap equation" to obtain the quasi-particle energies and the occupation numbers depending upon the Fermi energy λ.

$$\Delta_\alpha = -\frac{1}{4}\sum_\gamma \langle \alpha\bar{\alpha}|V^{\text{eff}}|\gamma\bar{\gamma}\rangle \frac{\Delta_\gamma}{E_\gamma}, \tag{16}$$

$$E_\alpha = \sqrt{(\varepsilon_\alpha - \lambda)^2 + \Delta_\alpha^2}, \qquad u_\alpha^2 = \frac{1}{2}\left(1 + \frac{\varepsilon_\alpha - \lambda}{E_\alpha}\right), \qquad v_\alpha^2 = \frac{1}{2}\left(1 - \frac{\varepsilon_\alpha - \lambda}{E_\alpha}\right). \tag{17}$$

The BCS approximation makes the numerical calculations of even–even nuclei much easier. However, it fails for odd nuclei and more generally in cases where the time-reversal invariance is broken. Nuclei far from stability and especially close to the proton or neutron drip lines (where the corresponding Fermi energy comes approaches to zero) require also a full HFB treatment, because the BCS approximation fails again when quasi-particle states couple HF states with positive energies [30,39–41].

Actually the HFB method, or its BCS approximation, needs an effective interaction to calculate the Δ pairing field (Eqs. (14) and (16)). In case of a finite range effective interaction used in the particle-hole channel, i.e., to generate the HF mean field h, the same force is used in order to obtain a self-consistent treatment of the pairing correlations. This is the case of the Gogny force. With a zero range interaction, one could do the same [30]. However one usually uses a different force in the particle-particle channel: a seniority force or a zero range force with a volume [42] or a surface [43] form factor. The case of zero range effective forces needs a specific attention. Zero range in coordinate space corresponds to infinite range in momentum space, thus a finite window of pairing correlations activity has then to be defined around the Fermi energy to prevent unphysical divergences.

3.2. Near the drip lines: Hartree–Fock–Bogoliubov theory far from stability

3.2.1. Continuum effects

Close to the drip lines, nuclei are loosely bound and it is now known from experiment that exotic nuclei exhibit specific properties such as skins and halos. These phenomena are due to the unusual spatial extension of the wave functions and to the residual couplings between bound and scattering states. Therefore one has to pay a special attention to the resolution of the mean field equations and to work in a space which includes both bound and scattering states. This could be achieved by integrating the equations in a sufficiently large box for instance [30].

To illustrate the role of the single-particle continuum, we have built the following model for $s_{1/2}$ neutron orbitals. We start from the spherical HFB problem in coordinate representation:

$$\begin{pmatrix} h(\boldsymbol{r}) & \Delta(\boldsymbol{r}) \\ -\Delta(\boldsymbol{r})^* & -h^*(\boldsymbol{r}) \end{pmatrix} \begin{pmatrix} U(\boldsymbol{r}) \\ V(\boldsymbol{r}) \end{pmatrix} = \begin{pmatrix} E+\lambda & 0 \\ 0 & E-\lambda \end{pmatrix} \begin{pmatrix} U(\boldsymbol{r}) \\ V(\boldsymbol{r}) \end{pmatrix}. \tag{18}$$

Instead of solving this system in a fully self consistent way, we replace the diagonal part of the HF mean field by a fixed model potential for which single-particle energies and wave functions are analytically known for $s_{1/2}$ states [41]. The pairing field $\Delta(\boldsymbol{r})$ is computed self-consistently using a simple zero-range interaction. This model allows to investigate the effect of the coupling between bound and scattering single-particle states in different cases. The potential parameters are adjusted in order to study an hypothetical nucleus with $N \lessapprox 82$ with a $3s_{1/2}$ state which is either resonant (a), virtual (b) or loosely bound (c) (see Table 1). The virtual state correspond to a pole of the S matrix on the negative energy axis (as it is for a bound state), but the corresponding wave function is not square integrable.

When the system (18) is solved we construct the particle density ρ from the V component of the quasi-particle wave functions. The diagonalization of ρ yields the canonical states which govern the pairing properties of the system [3]:

$$\rho\psi_n = v_n^2 \psi_n, \tag{19}$$

the canonical energies ε_n are defined as the diagonal matrix elements of the HF field h in the canonical basis.

Table 1
Properties of the HFB solutions in the three cases listed in the text. The neutron Fermi energies λ_N and pairing gaps $\langle \Delta_N \rangle$ are given in keV. The energies ε (in keV) and occupation numbers v^2 of the $3s_{1/2}$ canonical states are also reported

Case	λ_N	$\langle \Delta_N \rangle$	$\varepsilon_{3s_{1/2}}$	$v^2_{3s_{1/2}}$
(a)	−314	1146	2148	0.0321
(b)	−348	1298	1043	0.1002
(c)	−488	1421	390	0.2083

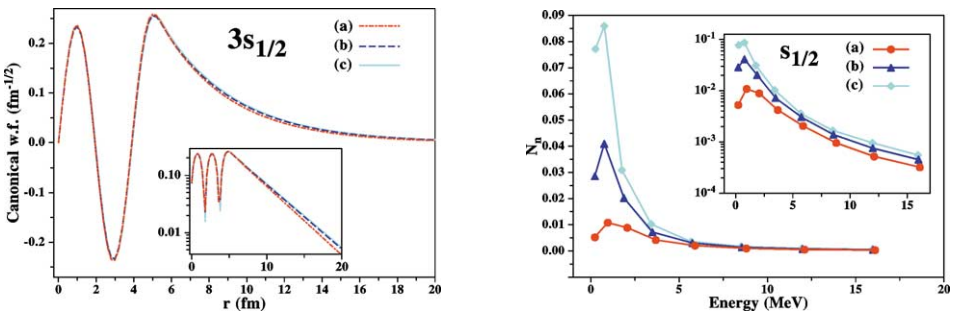

Fig. 6. Left: canonical wave functions of the $3s_{1/2}$ state for the three cases discussed in the text: resonant (a), virtual (b) and loosely bound (c) $3s_{1/2}$ state in the fixed HF potential. The inset represent the modulus of the same wave functions in logarithmic scale.
Right: norms N_n of the lower component of the quasi-particle wave functions as a function of the energy for the same three cases (a), (b) and (c). The insert shows the same quantities in logarithmic scale. See K. Bennaceur et al. [41] for more details.

As can be seen in Fig. 6, the canonical $3s_{1/2}$ wave function seems to be unaffected by the change in the HF spectrum from (a) to (c). We see on Table 1 that the overall pairing intensity $\langle \Delta_N \rangle$ increases by about 300 keV. This evolution is explained by the change in energy and the increase of the $3s_{1/2}$ occupation. Apart from this increase of pairing intensity, there is no other change in the pairing properties as the $3s_{1/2}$ state becomes bound.

On the right part of Fig. 6, we show the norm of the lower HFB component $N_n = \int V_n^2(r)\,\mathrm{d}\boldsymbol{r}$ which enter in the particle density ρ. Since the lower HFB components are not mutually orthogonal, N_n cannot be associated with occupation probabilities. The v^2 canonical occupation factors do play such a role, because the canonical states form a basis. Comparing the values of N_n (Fig. 6) and v^2 (Table 1), one sees that the canonical $3s_{1/2}$ collects all the occupation strength of the quasi-particle states in the lower energy continuum. In the case (c), i.e., when the single-particle $3s_{1/2}$ state is bound, the corresponding canonical state is partly built on it. The low energy continuum plays the role of the loosely bound states when this later is absent, in the cases (a) and (b). In every case all quasi-particle states below about 5 MeV contribute significantly to v^2.

The situation with the loosely bound state is not very different of the one meet close to the stability where BCS approaches can be used, apart from the long tail of the wave function. On the other hand, when the single-particle $3s_{1/2}$ state is virtual or resonant, no single-particle state could have been easily chosen in the HF spectrum to build the density and canonical states. Despite of this deep difference in the HF spectrum, we see that the canonical states remain essentially the same. This illustrate the important role which can be played by the $s_{1/2}$ continuum which has to be taken as a real continuum (discretized, if needed).

3.2.2. Quenching of the shell effects

The validity of the effective interaction far from stability is still an open problem. In particular, the structure of the spin-orbit force, the pairing part of the interaction and their interplay requires further studies. Possible modifications of the effective interaction will have consequences on all observables. For instance, it is known that shell gaps and magic numbers vary with deformation, a similar behavior might by expected as a function of isospin.

As an illustration we show in Fig. 7 the evolution of two semi magic systems: the case of $Z = 40$ isotopes (Zirconium) as a function of N, and the case of $N = 28$ isotones as a function of Z. Calculations have been made with the SLy4 interaction [31] in the spherical HFB approximation. In the first case, $N = 28$ isotones, we see that the gap between the $1f_{7/2}$ and the $2p_{3/2}$ states decreases from 5 MeV for proton rich nuclei to about 2 MeV close to the neutron drip line. The robustness of the $1f_{7/2}$ shell closure is then largely reduced and dynamical effect, beyond the mean field approximation, can mix configurations with particle-hole excitations. As shown on the right-hand side of Fig. 7, the calculation predicts that the $Z = 40$ magic number does not collapse in very proton rich nuclei, on the contrary, the $2p_{1/2}$–$1g_{9/2}$ gap varies from 2.5 to 3 MeV.

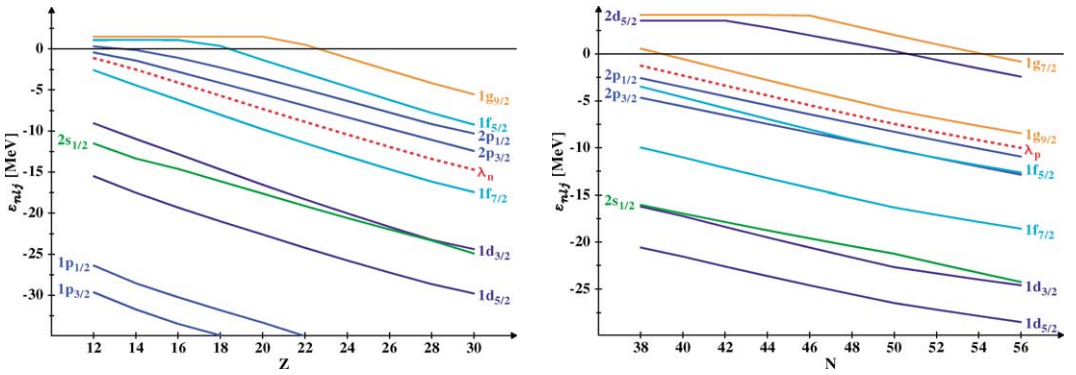

Fig. 7. Single-particle HF energies given by SLy4 for the isotonic chain $N = 28$ (left) and for the isotopic chain of Zirconium (right). The dashed lines represent the corresponding Fermi energies λ.

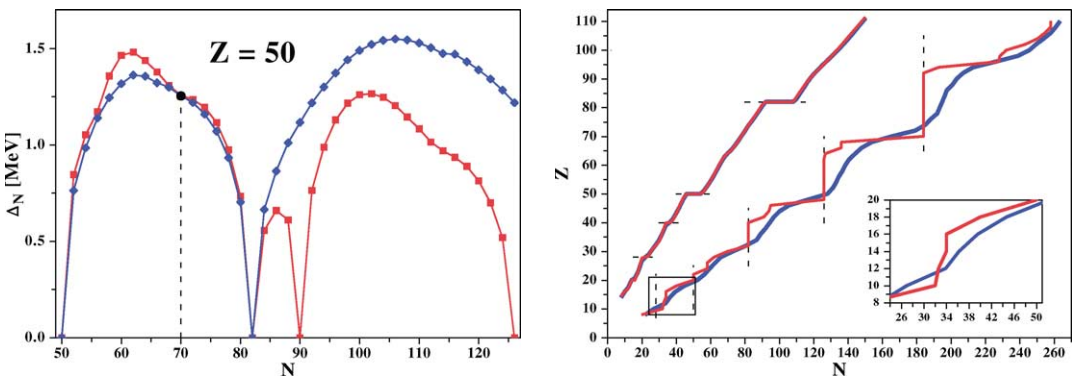

Fig. 8. Results of spherical HFB calculations with the SLy4 effective force in the *ph* channel and with a volume (red) or a surface (blue) pairing interaction [40,51] in the *pp* channel. Left: neutron gap Δ_N for Tin isotopes. The strength of the two pairing interactions have been tuned to give a neutron gap around 1.250 MeV in ^{120}Sn. Right: proton and neutron drip lines obtained with the same ingredients. The inset shows the region $28 < N < 50$ where the volume pairing predicts a shell effect for $N = 32$.

By looking at the behavior of the $2d_{5/2}$ and $1g_{7/2}$ states, we see that the states remain well confined inside the nucleus up to at least 2.5 MeV. So the properties of the proton rich nuclei are mostly unchanged when approaching the drip line since the density of state around the Fermi energy and the structure of the wave functions are not strongly affected by the continuum.

The calculations done here have been made using the SLy4 interaction which predicts different possible evolutions for the magic gaps as a function of the isospin, but further investigations and comparison with experiments have to be done to determine if such an interaction has a predictive power far from the stability. The vicinity of the continuum can increase the density of state above the Fermi surface and then strongly modify the pairing properties of the nucleus, so can the spin-orbit part of the interaction. The latter is probably the part of the interaction which has to be studied with the greater attention in the future development of microscopic mean field models.

3.2.3. Pairing interaction near the drip lines

Our knowledge of the effective interaction in the pairing channel is rather scarce. Its details are not decisive for nuclei close to the valley of stability but they lead to completely different predictions for neutron rich nuclei. This is illustrated by Fig. 8 which presents spherical HFB calculations performed either with a volume type or a surface density dependent pairing interaction. We see on the left part of the figure that the mean neutron gap Δ_N does not depend too much upon the choice of the pairing interaction for nuclei with $Z \leqslant N \leqslant 84$. On the other hand, the behavior is dramatically different for $N > 84$ with a disappearance of pairing for $N = 90$ and $N = 126$ in the case of the volume type pairing.

The right part of the figure shows the $\lambda_n = 0$ and $\lambda_p = 0$ contours which correspond roughly to the line of particle emission, i.e., the neutron and proton drip lines respectively. The proton drip line is almost insensitive to the nature of the pairing interaction while the position of the drip line and the shell effects are completely different on the neutron rich side. This

sensitivity to the details of the pairing interaction in the particle–particle (*pp*) channel is due to the important density of states around the Fermi surface in neutron rich nuclei. The nature of the effective pairing interaction is still subject of debate, see for example the discussions in [44,45].

3.3. Beyond the mean field approximation: the Generator Coordinate Method

3.3.1. The GCM method

The HFB/HFBCS method does not always generate a good wave function for the ground state of the studied nucleus. This is illustrated on Fig. 1 for the Magnesium isotopes where the wave functions of the absolute minima obtained in HFBCS calculations can be sometimes degenerated. The ^{20}Mg nucleus appears to be rigid along the Q collective coordinate and the spherical solution ($Q = 0$) will give a good wave function consistently with the $N = 8$ neutron magic number for this isotope. One can also expect a well deformed solution for the ^{24}Mg and the $^{36–40}$Mg nuclei even if for the latter a competition does exist between a first prolate solution and an second oblate one. The situation is less favorable for the ^{22}Mg, $^{26–30}$Mg and ^{34}Mg nuclei which present a large softness as a function of quadrupole deformation. For the ^{28}Mg nucleus, the wave functions obtained for $Q = -0.5b$ to $Q = 0.5b$ are quasi degenerated and the ground state wave function of this nucleus will be a superposition of solutions obtained for different values of Q.

The Generator Coordinate Method (GCM) [46] realizes such a mixing from a set of wave functions corresponding to one or several collective coordinates [46,47]. The most refined version of the GCM [48] runs in two steps. The first one consists to start from a set of HFBCSLN wave functions $\{|\Phi(q)\rangle\}$ – associated to a collective coordinate q – and to project them onto correct particle numbers by means of the projector $\widehat{P}_{N_0}$ [49]:

$$\widehat{P}_{N_0} = \frac{1}{\pi} \int_{-\pi/2}^{\pi/2} \mathrm{d}\phi \, \mathrm{e}^{\mathrm{i}\phi(\widehat{N}-N_0)}, \tag{20}$$

where the integral over the ϕ gauge angle is performed with the weight factor $\mathrm{e}^{-\mathrm{i}\phi N_0}$. From the mean field wave functions $\{|\Phi(q)\rangle\}$ we build the nonorthogonal projected collective basis $\{|\Phi_{N_0}(q)\rangle\}$ as:

$$\big|\Phi_{N_0}(q)\big\rangle = \widehat{P}_{N_0}\big|\Phi(q)\big\rangle. \tag{21}$$

In this basis the expectation value $\mathcal{E}(q)$ of the Hamiltonian of the nucleus is the projected deformation energy:

$$\mathcal{E}(q) = \frac{\langle\Phi_{N_0}(q)|\widehat{H}|\Phi_{N_0}(q)\rangle}{\langle\Phi_{N_0}(q)|\Phi_{N_0}(q)\rangle} = \frac{\langle\Phi(q)|\widehat{H}\,\widehat{P}_{N_0}|\Phi(q)\rangle}{\langle\Phi(q)|\widehat{P}_{N_0}|\Phi(q)\rangle}. \tag{22}$$

Several such potential energy surfaces have been presented in the Fig. 2 for some $N = Z$ nuclei.

In the second step one considers a more general N-body wave function defined as a linear superposition of projected HFBCSLN states with a weight function $f_j(q)$:

$$|\Psi_j\rangle = \int \mathrm{d}q f_j(q)\big|\Phi_{N_0}(q)\big\rangle, \tag{23}$$

where the label j recalls that several states $|\Psi_j\rangle$ are obtained corresponding to the correlated ground state and to the collective excited states. Within the GCM method, the weight function is determined by a variation of the total energy E_j with respect to $f_j^*(q)$:

$$E_j = \frac{\langle\Psi_j|\widehat{H}|\Psi_j\rangle}{\langle\Psi_j|\Psi_j\rangle}. \tag{24}$$

This leads to the Hill–Wheeler equations [46]. Due to particle number projection, the kernels $\mathcal{I}$, $\mathcal{N}$ and $\mathcal{H}$ of the integral operators entering these equations take the following form [48]:

$$\begin{pmatrix} \mathcal{I}(q',q) \\ \mathcal{N}(q',q) \\ \mathcal{H}(q',q) \end{pmatrix} = \frac{1}{\pi} \int_{-\pi/2}^{\pi/2} \mathrm{d}\phi \, \mathrm{e}^{-\mathrm{i}\phi N_0}\big\langle\Phi(q')\big| \begin{pmatrix} \hat{1} \\ \widehat{N} \\ \widehat{H} \end{pmatrix} \mathrm{e}^{\mathrm{i}\phi\widehat{N}}\big|\Phi(q)\big\rangle. \tag{25}$$

The evaluation of these (q', q) dependent kernels is the most time consuming numerical part and is also the main reason which limits the method to one or two collective variables. They involve a double integral (for N and Z respectively) of matrix elements of one-body and two-body operators between all possible states of the collective basis $\{|\Phi(q)\rangle\}$ [47]. Other kernels involving multipole moment operators associated with various one-body observables are also needed for the computation of all the properties of the collective GCM states.

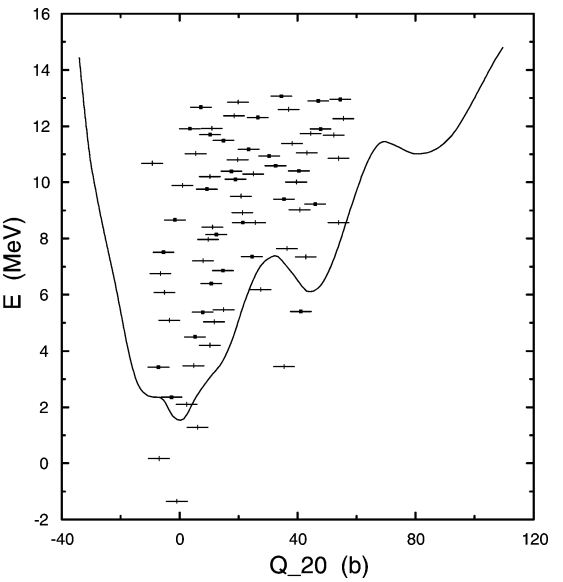

Fig. 9. Energy of GCM collective states of the ^{194}Pb nucleus: levels are represented by short horizontal bars located at eigen energies and average values of the quadrupole moment Q_{20}. Negative parity states are represented with a black dot. The static HFBCS axial quadrupole deformation energy (solid curve) is given as a reference. The origin of the energies is fixed at the energy of the GCM ground state without the octupole degree of freedom. See Meyer et al. [13] for more details.

3.3.2. Quadrupole and octupole mixing in ^{194}Pb

Quadrupole or octupole vibrations have been extensively investigated using the GCM method and we will present here two examples. The first one concerns exotic shapes such as superdeformed (SD) or hyperdeformed (HD) shapes as shown on Fig. 9 for the ^{194}Pb nucleus. The HFBCS calculations performed along the quadrupole and octupole moments have exhibited several minima (Fig. 3) and it is necessary to investigated their robustness against Q_{20} and/or Q_{30} dynamical vibrations. Fig. 9 shows the result of a two dimensional GCM analysis of the static potential energy surface previously shown on Fig. 3. Since the Q_{30} moment breaks the z-parity the GCM generates two independent positive and negative parity spectra. These GCM states have no well-defined angular momentum and can be considered as a band head of a rotational band. We obtain a positive parity state for the ground state of the ^{194}Pb and some positive and negative parity excited states which we interpret as quadrupole and octupole multi phonon excitations. In the second minimum there are also a positive parity SD state as well as a negative one. Let us recall that rotational bands built an these states have been experimentally seen [61,63] down to very low spins. On the contrary, the HD third minimum is not deep enough to stabilize a HD GCM state and no such HD state has been observed. Fig. 9 gives an estimation of the energy gain resulting from the mixing of quadrupole and octupole vibrations, namely around 1.7 MeV for the spherical ground state and around 2.5 MeV for both SD states.

3.3.3. Charge radii of Tin isotopes

The second example is a GCM analysis of the effect of quadrupole vibrations on the charge radii of Tin isotopes. HFB as well as HFBCS calculations have been performed along the Tin isotopic serie from the ^{100}Sn nucleus up to the ^{168}Sn nucleus, i.e., roughly from the proton to the neutron drip lines. Recent experimental progresses have been made by F. Leblanc et al. and the COMPLIS collaboration [64] to obtain the charge radii up to the doubly magic ^{132}Sn nucleus. Fig. 10 shows the result of HFB/HFBCS calculations of Tin charge radii. First one sees that the HFB versus HFBCS treatment of pairing correlations does not influence significantly the results, neither does the particle number projection. On the contrary the dynamical effects of quadrupole vibrations within a GCM calculation allow to explain a large part of the difference between HFB/HFBCS calculations and the experimental data. These effects can be also exhibited on the binding energies of these nuclei as shown on the right part of Fig. 10 where the energy difference between the N/Z projected HFBCS and the GCM solutions for the ground states are plotted as a function of A. The quadrupole vibrations occur to be minimum for the doubly magic ^{100}Sn and ^{132}Sn nuclei and maximum in between.

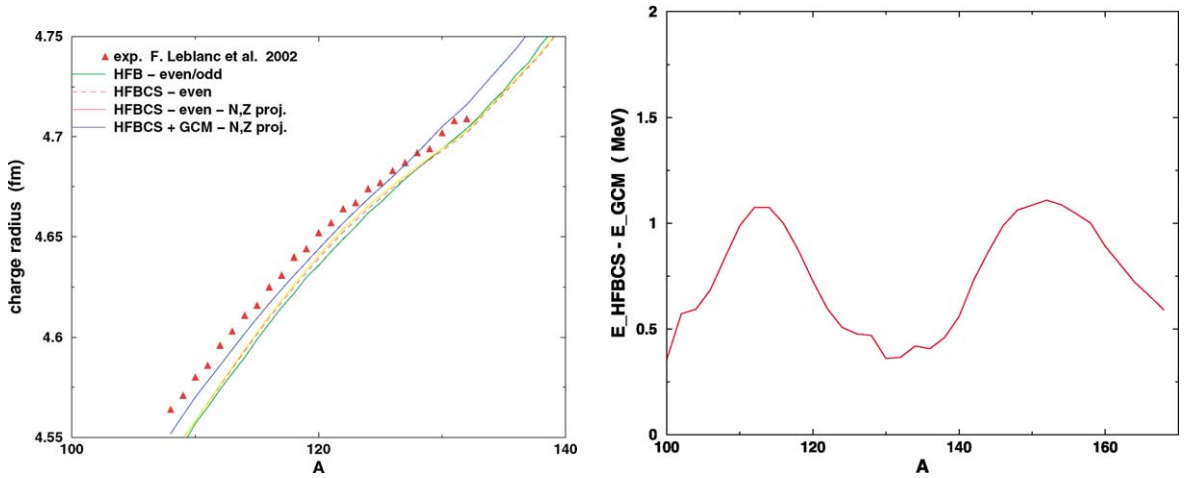

Fig. 10. Left: charge r.m.s. radii for Tin isotopes. Green curve: HFB results for even–even and odd isotopes; dot red curve: HFBCS results for even–even isotopes; full red curve: N, Z projected HFBCS results; blue curve: N, Z projected HFBCS plus quadrupole GCM results. The experimental charge radii (red triangles) are from F. Leblanc et al. [64]. Right: energy difference between the N, Z projected-HFBCS and GCM solutions. The SLy4 effective interaction is used.

4. Conclusions and outlook

The general assumptions of microscopic mean field theories have been presented and illustrated by some examples of properties of nuclei far from stability. Nuclear correlations beyond mean field have been also investigated especially pairing which is a key ingredient to obtain correct wave functions for open shell nuclei. The treatment of these pairing correlations through the Hartree–Fock–Bogoliubov formalism has been discussed together with the question of the coupling to the continuum for these exotic nuclei where the Fermi energy vanishes. Other methods to go beyond the mean field approximation have been exposed such as the Generator Coordinate Method which enable to construct wave function for multi configurations. Projection onto particle number has been implemented to obtain wave functions with a good nucleon numbers.

Moreover the concept of effective interaction was presented in the context nonrelativistic mean field theories. Some basic features of these effective forces such as density dependence have been also discussed for the phenomenological Gogny or Skyrme interactions. The most accurate density dependence of such an effective force still remains an open question [50] and the new effective interactions recently proposed based on properties of neutron stars seem to be a first possible answer. Further improvements of these forces are in progress particularly concerning a generalized density dependence and the use of new experimental data on charge or neutron radii in connection with astrophysics.

The $T = 1$ pairing correlations – neutron–neutron or proton–proton – are the only one to be taken into account in the HFB formalism which are neglecting the neutron–proton (n–p) pairing. Recent works [52] investigate these correlations in light $N = Z$ nuclei and tries thereby to give an accurate microscopic explanation of the Wigner energy [53]. It has not been yet clearly proved unambiguously that this gain in energy in $N = Z$ nuclei is fully bound to this n–p pairing [54], other correlations beyond the mean field approximation may give a significant contribution [55].

The main ingredient of a *reasonable effective NN interaction* is a correct description of the bulk properties of the nuclear fluid: equilibrium density, binding energy per nucleon, compression modulus, effective mass. The connections between these properties and the parameters of the nuclear equation of state (EOS) or those of the effective force are under control through collective phenomena such as giant resonances generally more sensitive to the global behavior of the nuclear medium than local shell effects. Isovector properties such as symmetry energy, isovector effective mass or pure neutron matter EOS are also connected to the fundamental parameters of the effective force and could be studied through a better experimental knowledge of collective modes in extreme conditions [56]. Some exotic modes “pigmy” mode, “soft dipole” mode [56], characteristics of nuclei with large neutron skin have been theoretically predicted and a systematic experimental research of these collectives modes should be now possible with new generation of radioactive beams.

In addition to the nuclear masses, the charge and neutron radii are also building blocks in the construction of effective forces. In this respect, recent experimental measurements of charge radii along long isotopic series [64] are quite relevant. If it were possible to obtain accurate measurements of neutron distributions in order to extract neutron radii [57,58] and the size of neutron skins [59,60], one would have at disposal a complete set of experimental constraints for a better understanding of an effective interaction in extreme conditions of isospin.

The predictions concerning the evolution of the shell effects in extreme conditions of deformation and/or spin was certainly one of the greatest successes of the mean field theories for fission isomers as well as for the superdeformation phenomena and the high spin physics [61]. It is also important to investigate the behavior of these shell structures in extreme conditions of isospin, as well as for super heavy nuclei for which available predictions differ between relativistic and nonrelativistic mean field theories. The evolution of these shell effects for exotic nuclei [62] is in close connection with the spin-orbit term of the effective force and a better parametrization of this term in relation with relativistic theories has still to be done. Experimental results concerning single-particle spectra for long isotopic series of spherical nuclei such as Nickel or Tin isotopes should enable a better control of this degree of freedom in theoretical models.

The results obtained within microscopic – nonrelativistic as well as relativistic – mean field theories make these theoretical models out to be a main piece to investigate the structure of atomic nuclei. The reliability of these approaches, mainly estimated for their prediction power, constitutes the starting point of numerous experimental progress, indeed of plans for future accelerators dedicated to the study of nuclei under extreme conditions. However it is fundamental never to forget that all these models use some basic ingredients, an effective interaction for instance, for which one has to check the pertinence towards the formulated problem. The progress of these approaches is closely bound to the progress made to improve these effective forces, this latter itself dependent of new experimental data.

Acknowledgements

We would like to thank Bertrand Cochet, Jean-François Berger, Jacek Dobaczewski, Thomas Duguet and Paul-Henri Heenen for illuminating discussions and several fundamental comments which have contributed to clarify some points of the discussion. Thanks also to François Leblanc for communication of experimental charge radii before publication. Special thanks to Florence Chouri for a careful reading of the manuscript. The numerous meetings organized by the GDR *Exotic Nuclei* have been opening a lot of debates both on experimental and theoretical points related to the new field of nuclear structure.

References

[1] P. Ring, contribution to this volume.
[2] Special issue on Radioactive Nuclear Beams dedicated to the memory of Jerry D. Garrett, Nucl. Phys. A 693 (2001) 1.
[3] P. Ring, P. Schuck, The Nuclear Many-Body Problem, Spinger-Verlag, Berlin, 1980.
[4] G. Bertsch, Z. Phys. A 289 (1978) 103.
[5] Ph. Quentin, H. Flocard, Annu. Rev. Nucl. Part. Sci. 28 (1978) 523.
[6] P. Bonche, H. Flocard, P.-H. Heenen, S.J. Krieger, M.S. Weiss, Nucl. Phys. A 443 (1985) 39.
[7] P. Bonche, S.J. Krieger, P. Quentin, M.S. Weiss, J. Meyer, M. Meyer, N. Redon, H. Flocard, P.-H. Heenen, Nucl. Phys. A 500 (1989) 308; S.J. Krieger, P. Bonche, M.S. Weiss, J. Meyer, H. Flocard, P.-H. Heenen, Nucl. Phys. A 542 (1992) 43.
[8] M. Girod, B. Grammaticos, Phys. Rev. C 27 (1983) 2317.
[9] M. Girod, J.P. Delaroche, D. Gogny, J.F. Berger, Phys. Rev. Lett. 62 (1989) 2452.
[10] S. Aberg, H. Flocard, W. Nazarewicz, Annu. Rev. Nucl. Part. Sci. 40 (1990) 439.
[11] J.L. Wood, K. Heyde, W. Nazarewicz, M. Huyse, P. Van Duppen, Phys. Rep. 215 (1992) 101.
[12] J. Terasaki, H. Flocard, P.-H. Heenen, P. Bonche, Nucl. Phys. A 621 (1997) 706.
[13] J. Meyer, P. Bonche, M.S. Weiss, J. Dobaczewski, H. Flocard, P.-H. Heenen, Nucl. Phys. A 588 (1995) 597.
[14] B. ter Haar, R. Malfliet, Phys. Rep. 149 (1987) 207.
[15] D. Vautherin, Nuclear Physics of Hot Dense Matter, in: NATO Adv. Study Inst. Supernovae, Les Houches, France, 1990.
[16] J.W. Negele, Rev. Mod. Phys. 54 (1982) 913.
[17] M. Hjorth-Jensen, T.T.S. Kuo, E. Osnes, Phys. Rep. 261 (1995) 125.
[18] M. Baldo, Nuclear Methods and the Nuclear Equation of State, in: Int. Review of Nuclear Physics, Vol. 9, World Scientific, Singapore, 1999.
[19] H. Müther, Prog. Part. Nucl. Phys. 14 (1985) 125;
H. Müther, Prog. Part. Nucl. Phys. 17 (1986) 97;
H. Müther, Prog. Part. Nucl. Phys. 30 (1993) 1.
[20] J.W. Negele, Phys. Rev. C 1 (1970) 1260.
[21] D.W.L. Sprung, P.K. Banerjee, Nucl. Phys. A 168 (1971) 273;
D.W.L. Sprung, Nucl. Phys. A 182 (1972) 97;
X. Campi, D.W. Sprung, Nucl. Phys. A 194 (1972) 401.
[22] S.C. Pieper, R.B. Wiringa, V.R. Pandharipande, Phys. Rev. C 46 (1992) 1741.
[23] H.S. Köhler, Nucl. Phys. A 162 (1971) 385;
H.S. Köhler, Nucl. Phys. A 170 (1971) 88.
[24] J. Dechargé, D. Gogny, Phys. Rev. C 21 (1980) 1568.

[25] J.F. Berger, M. Girod, D. Gogny, Nucl. Phys. A 502 (1989) 85c.
[26] T.H.R. Skyrme, Philos. Mag. 1 (1956) 1043;
T.H.R. Skyrme, Nucl. Phys. 9 (1959) 615.
[27] D. Vautherin, D.M. Brink, Phys. Rev. C 3 (1972) 626.
[28] M. Beiner, H. Flocard, Nguyen Van Giai, P. Quentin, Nucl. Phys. A 238 (1975) 29.
[29] J. Bartel, P. Quentin, M. Brack, C. Guet, H.-B. Hakansson, Nucl. Phys. A 386 (1982) 79.
[30] J. Dobaczewski, H. Flocard, J. Treiner, Nucl. Phys. A 422 (1984) 103.
[31] E. Chabanat, P. Bonche, P. Haensel, J. Meyer, R. Schaeffer, Nucl. Phys. A 627 (1997) 710;
E. Chabanat, P. Bonche, P. Haensel, J. Meyer, R. Schaeffer, Nucl. Phys. A 635 (1998) 231;
E. Chabanat, P. Bonche, P. Haensel, J. Meyer, R. Schaeffer, Nucl. Phys. A 643 (1998) 441.
[32] F. Buchinger, J.E. Crawford, A.K. Dutta, J.M. Pearson, F. Tondeur, Phys. Rev. C 49 (1994) 1402.
[33] J.W. Negele, D. Vautherin, Phys. Rev. C 5 (1972) 1472;
J.W. Negele, D. Vautherin, Phys. Rev. C 11 (1975) 1031.
[34] C.J. Batty, E. Friedman, H.J. Gils, H. Rebel, in: J.W. Negele, M. Vogt (Eds.), Adv. Nucl. Phys., Vol. 19, Plenum Press, New York, 1989.
[35] J. Bardeen, L.N. Cooper, J.R. Schrieffer, Phys. Rev. 108 (1957) 1175.
[36] H.J. Lipkin, Ann. Phys. (NY) 12 (1960) 425;
Y. Nogami, Phys. Rev. B 134 (1964) 313;
A. Kamlah, Z. Phys. 216 (1968) 52.
[37] Ph. Quentin, N. Redon, J. Meyer, M. Meyer, Phys. Rev. C 41 (1990) 341.
[38] P.-H. Heenen, A. Valor, M. Bender, P. Bonche, H. Flocard, Eur. Phys. J. A 11 (2001) 393.
[39] W. Nazarewicz, J. Dobaczewski, T.R. Werner, J.A. Maruhn, P.-G. Reinhard, K. Rutz, C.R. Chinn, A.S. Umar, M.R. Strayer, Phys. Rev. C 53 (1996) 740;
J. Dobaczewski, W. Nazarewicz, T.R. Werner, Z. Phys. A 354 (1996) 27.
[40] J. Dobaczewski, W. Nazarewicz, T.R. Werner, J.-F. Berger, C.R. Chinn, J. Dechargé, Phys. Rev. C 53 (1996) 2809.
[41] K. Bennaceur, J. Dobaczewski, M. Płoszajczak, Phys. Rev. C 60 (1999) 034308.
[42] F. Tondeur, Nucl. Phys. A 315 (1979) 353;
S.J. Krieger, P. Bonche, H. Flocard, P. Quentin, M.S. Weiss, Nucl. Phys. A 517 (1990) 275.
[43] R.R. Chasman, Phys. Rev. C 14 (1976) 1935;
N. Tajima, P. Bonche, H. Flocard, P.-H. Heenen, M.S. Weiss, Nucl. Phys. A 551 (1993) 434;
J. Terasaki, P.-H. Heenen, P. Bonche, J. Dobaczewski, H. Flocard, Nucl. Phys. A 593 (1995) 1.
[44] J. Dobaczewski, W. Nazarewicz, M.V. Stoitsov, 3rd Int. Conf. on Exotic Nuclei and Atomic Masses, ENAM 2001, Hameenlinna, Finlande, 2001, Eur. Phys. J. A 15 (2002) 21.
[45] S.A. Fayans, D. Zawischa, Phys. Lett. B 383 (1996) 19;
S.A. Fayans, S.V. Tolokonnikov, E.L. Trykov, D. Zawischa, Nucl. Phys. A 676 (2000) 49.
[46] D.L. Hill, J.A. Wheeler, Phys. Rev. 89 (1953) 1102.
[47] P. Bonche, J. Dobaczewski, H. Flocard, P.-H. Heenen, J. Meyer, Nucl. Phys. A 510 (1990) 466.
[48] P.-H. Heenen, A. Valor, M. Bender, P. Bonche, H. Flocard, Eur. Phys. J. A 11 (2001) 393;
M. Bender, P.-H. Heenen, P.-G. Reinhard, Rev. Mod. Phys. 75 (2003) 121.
[49] P.-H. Heenen, P. Bonche, J. Dobaczewski, H. Flocard, Nucl. Phys. A 561 (1993) 367.
[50] Th. Duguet, nucl-th/0210051;
Th. Duguet, P. Bonche, nucl-th/0210055;
Th. Duguet, P. Bonche, nucl-th/0210057.
[51] S.T. Belyaev, A.V. Smirnov, S.V. Tolokonnikov, S.A. Fayans, Soviet J. Nucl. Phys. 45 (1987) 783.
[52] J. Engel, K. Langanke, P. Vogel, Phys. Lett. B 389 (1996) 211;
A. Goodman, Phys. Rev. C 58 (1998) R3051;
W. Satuła, R.A. Wyss, Phys. Lett. B 393 (1997) 1;
W. Satuła, R.A. Wyss, Phys. Rev. Lett. 87 (2001) 052504;
P. Vogel, Nucl. Phys. A 662 (2000) 148.
[53] W. Satuła, D.J. Dean, J. Gary, S. Mizutori, W. Nazarewicz, Phys. Lett. B 407 (1997) 103.
[54] W. Satuła, Int. Conf. Nuclear Structure '98, Gatlinburg, USA, 1998, nucl-th/9809089.
[55] W. Satuła, R.A. Wyss, Acta Phys. Pol. B 32 (2001) 2441;
W. Satuła, R.A. Wyss, Phys. Rev. Lett. 86 (2001) 4488;
S. Glowacz, W. Satuła, R.A. Wyss, nucl-th/0212086.
[56] T. Suzuki, H. Sagawa, Prog. Part. Nucl. Phys. 46 (2001) 135;
H. Sagawa, H. Esbensen, Nucl. Phys. A 693 (2001) 448.
[57] W.R. Gibbs, J.-P. Dedonder, Phys. Rev. C 46 (1992) 1825;
C.J. Horowitz, Comptes-Rendus de la Qubec Intersections Conference, nucl-th/0010010;
C.J. Horowitz, S.J. Pollock, P.A. Souder, R. Michaels, Phys. Rev. C 63 (2001) 025501.
[58] R. Michaels, P.A. Souder, G.M. Urciuoli, Spokesmen, Proposal to Jefferson Laboratory.
[59] N. Fukunishi, T. Otsuka, I. Tanihata, Phys. Rev. C 48 (1993) 1648.
[60] S. Karataglidis, K. Amos, B.A. Brown, P.K. Deb, Phys. Rev. C 65 (2002) 044306.
[61] M. Meyer, J.-P. Vivien, Ann. Phys. France 17 (1992) 11.

[62] H. Grawe, M. Lewitowicz, Nucl. Phys. A 693 (2001) 116.
[63] B. Crowell, et al., Phys. Lett. B 333 (1994) 320;
B. Crowell, et al., Phys. Rev. C 51 (1995) R1599;
A.N. Wilson, et al., Phys. Rev. C 54 (1996) 559;
P. Fallon, et al., Phys. Rev. C 55 (1997) R999.
[64] F. Le Blanc, et al., Proceedings of the Int. Conf. on Exotic Nuclei and Atomic Masses, ENAM 2001, Haemeenlinna, Finland, July 2001, Eur. Phys. J. A 15 (2002) 49;
F. Le Blanc, et al., in: Nuclear Physics at Border Line, World Scientific, Singapore, 2002;
F. Le Blanc, et al., Proceedings of the Int. Conf. on Nuclear Physics at Border Lines, Lipari Islands, Italy, May 2001;
F. Leblanc, private communication, 2002.